Article

Advancing CubeSats Capabilities: Ground-Based Calibration of Uvsq-Sat NG Satellite's NIR Spectrometer and Determination of the Extraterrestrial Solar Spectrum

Mustapha Meftah [1,*] , Christophe Dufour [1], David Bolsée [2], Lionel Van Laeken [2], Cannelle Clavier [1,3],
Amal Chandran [4], Loren Chang [5] , Alain Sarkissian [1] , Patrick Galopeau [1], Alain Hauchecorne [1] ,
Pierre-Richard Dahoo [1] , Luc Damé [1], André-Jean Vieau [1], Emmanuel Bertran [1], Pierre Gilbert [1], Fréderic Ferreira [1],
Jean-Luc Engler [1], Christophe Montaron [1], Antoine Mangin [3], Odile Hembise Fanton d'Andon [3], Nicolas Caignard [1],
Angèle Minet [1], Pierre Maso [1], Nuno Pereira [2], Étienne Brodu [2], Slimane Bekki [1], Catherine Billard [1]
and Philippe Keckhut [1]

1   Laboratoire Atmosphères, Observations Spatiales (LATMOS), Université de Versailles
    Saint-Quentin-en-Yvelines (UVSQ), Université Paris-Saclay (UPS), Sorbonne Université (SU),
    Centre National de la Recherche Scientifique (CNRS), 11 Boulevard d'Alembert, 78280 Guyancourt, France;
    christophe.dufour@latmos.ipsl.fr (C.D.); cannelle.clavier@latmos.ipsl.fr (C.C.);
    alain.sarkissian@latmos.ipsl.fr (A.S.); patrick.galopeau@latmos.ipsl.fr (P.G.);
    alain.hauchecorne@latmos.ipsl.fr (A.H.); pierre-richard.dahoo@latmos.ipsl.fr (P.-R.D.);
    luc.dame@latmos.ipsl.fr (L.D.); andre-jean.vieau@latmos.ipsl.fr (A.-J.V.);
    emmanuel.bertran@latmos.ipsl.fr (E.B.); pierre.gilbert@latmos.ipsl.fr (P.G.);
    frederic.ferreira@latmos.ipsl.fr (F.F.); jean-luc.engler@latmos.ipsl.fr (J.-L.E.);
    christophe.montaron@latmos.ipsl.fr (C.M.); nicolas.caignard@latmos.ipsl.fr (N.C.);
    angele.minet@uvsq.fr (A.M.); pierre.maso@uvsq.fr (P.M.); slimane.bekki@latmos.ipsl.fr (S.B.);
    catherine.billard@uvsq.fr (C.B.); philippe.keckhut@latmos.ipsl.fr (P.K.)
2   Royal Belgian Institute for Space Aeronomy (BIRA-IASB), Ringlaan 3 Avenue Circulaire,
    1180 Brussels, Belgium; david.bolsee@aeronomie.be (D.B.); lionel.vanlaeken@aeronomie.be (L.V.L.);
    nuno.pereira@aeronomie.be (N.P.); etienne.brodu@aeronomie.be (É.B.)
3   ACRI-ST—CERGA, 10 Avenue Nicolas Copernic, 06130 Grasse, France; antoine.mangin@acri-st.fr (A.M.);
    oha@acri-st.fr (O.H.F.d.)
4   Laboratory for Atmospheric and Space Physics (LASP), University of Colorado, 1234 Innovation Dr.,
    Boulder, CO 80303, USA; amal.chandran@lasp.colorado.edu
5   Department of Space Science and Engineering, National Central University (NCU), 300 Zhongda Road,
    Zhongli District, Taoyuan City 320317, Taiwan; loren@g.ncu.edu.tw
*   Correspondence: mustapha.meftah@latmos.ipsl.fr; Tel.: +33-1-80-28-51-79

Abstract: Uvsq-Sat NG is a French 6U CubeSat ($10 \times 20 \times 30$ cm) of the International Satellite Program in Research and Education (INSPIRE) designed primarily for observing greenhouse gases (GHG) such as CO_2 and CH_4, measuring the Earth's radiation budget (ERB), and monitoring solar spectral irradiance (SSI) at the top-of-atmosphere (TOA). It epitomizes an advancement in CubeSat technology, showcasing its enhanced capabilities for comprehensive Earth observation. Scheduled for launch in 2025, the satellite carries a compact and miniaturized near-infrared (NIR) spectrometer capable of performing observations in both nadir and solar directions within the wavelength range of 1100 to 2000 nm, with a spectral resolution of 7 nm and a 0.15° field of view. This study outlines the preflight calibration process of the Uvsq-Sat NG NIR spectrometer (UNIS), with a focus on the spectral response function and the absolute calibration of the instrument. The absolute scale of the UNIS spectrometer was accurately calibrated with a quartz-halogen lamp featuring a coiled-coil tungsten filament, certified by the National Institute of Standards and Technology (NIST) as a standard of spectral irradiance. Furthermore, this study details the ground-based measurements of direct SSI through atmospheric NIR windows conducted with the UNIS spectrometer. The measurements were obtained at the Pommier site (45.54°N, 0.83°W) in Charentes–Maritimes (France) on 9 May 2024. The objective of these measurements was to verify the absolute calibration of the UNIS spectrometer conducted in the laboratory and to provide an extraterrestrial solar spectrum using the Langley-plot technique. By extrapolating the data to AirMass Zero (AM0), we obtained high-precision results that show excellent agreement with SOLAR-HRS and TSIS-1 HSRS solar spectra. At 1.6 μm, the SSI was

determined to be 238.59 ± 3.39 mW.m^{-2}.nm^{-1} (k = 2). These results demonstrate the accuracy and reliability of the UNIS spectrometer for both SSI observations and GHG measurements, providing a solid foundation for future orbital data collection and analysis.

1. Introduction

CubeSats have emerged as a revolutionary tool in space exploration and research, democratizing access to space by providing a cost-effective and scalable platform for a broad range of scientific, educational, and commercial applications. These miniature satellites, typically built to standard dimensions of multiples of 10 cm cubes (1U, 2U, 3U, 6U, etc.), have proven to be invaluable in advancing our understanding of Earth and beyond. These nimble satellites offer a cost-effective solution for detailed Earth observation, capable of deploying large constellations in Low Earth Orbit to achieve continuous and comprehensive global coverage. This approach marks a significant shift in how we monitor climate change, moving away from reliance on larger, singular satellites. CubeSats, with their short development cycles and low operational costs, enhance our ability to observe Earth's climate dynamically and with greater spatial resolution. By leveraging the coordinated deployment of multiple satellites, each equipped with specialized instruments and capable of agile maneuvering, this new satellite paradigm enhances real-time monitoring and significantly improves the frequency and quality of data collection. However, before deploying such constellations, it is essential to implement a pathfinder CubeSat mission to validate the approach.

We are, therefore, in the process of developing the Uvsq-Sat NG in-orbit demonstrator satellite, which carries a NIR spectrometer (Figure A1) [1] designed for observing greenhouse gases (GHG) such as CO_2 and CH_4, measuring the ERB, and monitoring SSI at the TOA. Thanks to the Uvsq-Sat NG NIR spectrometer (UNIS), we aim to conduct ground-based measurements of solar radiation at sea level in the range of 1100–2000 nm. One of the goals of these measurements is to verify the quality of the UNIS spectrometer calibration performed in the laboratory to ensure optimal preflight calibration. Additionally, we aim to determine the SSI at TOA using the Langley-plot technique and based on UNIS ground-based observations, with a particular focus at 1600 nm. Another of our goals is to repeat the SSI observations with the UNIS spectrometer in orbit in 2025 to obtain a direct solar spectrum at TOA and compare it with the values obtained on the ground in May 2024 (SSI at TOA using the Langley-plot technique). This will also involve verifying any changes between the preflight calibration and the operational conditions in space.

This manuscript, therefore, presents the preflight calibration process of the UNIS spectrometer and offers a new assessment of SSI based on ground-based observations. Section 2 provides the scientific objectives associated with ground-based solar measurements conducted using the UNIS spectrometer. Section 3 details the calibration conducted on the UNIS spectrometer. Section 4 outlines the methodology for obtaining the Uvsq-Sat NG extraterrestrial spectrum based on the Langley-plot technique. The results are presented and discussed in Section 5, followed by a concluding summary.

2. Scientific Objectives of the UNIS NIR Spectrometer Ground-Based Measurements

The solar spectrum [2–4] represents the distribution of electromagnetic radiation emitted by the Sun across various wavelengths, from gamma rays to radio waves, including ultraviolet (10–380 nm), visible (380–780 nm) and infrared (780 nm to 1 mm). It characterizes the activity of the Sun's outer layers, such as the photosphere, chromosphere, transition region, and corona. Accurately measuring the extraterrestrial solar spectrum and understanding the long-term evolution of solar spectral irradiance (SSI) provides insights into magnetic field processes, therefore enhancing our understanding of variability in

the Sun's outer regions. These measurements facilitate the determination of temperature, composition, and density in these regions and, more broadly, contribute to the validation of solar atmosphere models.

The direct measurements and accurate determinations of SSI offer numerous benefits beyond solar physics. For example, it provides essential data for understanding how the Earth system responds to solar spectral variability. Notably, SSI is a crucial input for understanding the Earth's radiation budget (ERB), as it helps to balance the incoming energy from the Sun and the outgoing thermal (longwave) and reflected (shortwave) energy from the Earth, which is essential for accurate climate modeling and energy transfer studies. In another context, precise knowledge of SSI, particularly in the near-infrared (NIR) range (780–3000 nm), is vital for calibrating and validating satellite instruments such as MicroCarb [4,5] and other observational platforms, ensuring reliable and consistent data across various missions. This is particularly true for the Uvsq-Sat NG mission, which requires an accurate knowledge of the NIR solar spectrum to process the data and retrieve atmospheric gas columns (CO_2, CH_4, O_2, H_2O) from its NIR spectrometer observations [1].

The Global Climate Observing System (GCOS) designates the top-of-atmosphere (TOA) incoming SSI as an essential climate variable (ECV). ECV data records are designed to offer reliable, traceable, observation-based evidence for a variety of applications, including monitoring and mitigating climate changes, adapting to new conditions, and attributing specific climate events [6]. Therefore, as the primary driver of meteorological processes through the absorption and scattering of radiation [7], it is essential to accurately constrain measurements of incoming SSI. However, determining its absolute level remains challenging [2], regardless of whether ground-based instruments, research aircraft (e.g., the pioneering SSI observations of Arvesen et al. [8]), or satellite-based instruments are used.

Before the advent of the space age, solar irradiance measurements were conducted from the Earth's surface using zero AirMass extrapolation techniques, also known as the Langley-plot technique, to derive the solar irradiance at TOA within selected atmospheric windows [9,10]. Over the past 23 years, SSI measurements have primarily utilized spectro-radiometers [11–17] to determine the solar spectrum in wavelength regions that are minimally affected by atmospheric absorption features. These ground-based measurements have been employed for atmospheric research and to validate existing solar extraterrestrial spectra obtained from space-based measurements or solar models. While ground-based measurements of solar irradiance must account for changing atmospheric conditions, they offer a significant advantage over space-based instruments by allowing recalibration and validation of traceability to International System of Units (SI) standards. To obtain excellent results, it is preferable to conduct SSI ground-based observations at high-altitude sites such as the Mauna Loa Observatory in Hawaii (3400 m above sea level), the Jungfraujoch Observatory in the Swiss Alps (3600 m), and the Izaña Atmospheric Observatory on the island of Tenerife (2373 m). However, such sites may not always be accessible for conducting instrument calibrations quickly and frequently. The SSI ground-based measurements have several other disadvantages, such as a limitation in the range of observed wavelengths (atmospheric window). Over long periods, the stability of radiometers may not be reliable, potentially causing errors in TOA irradiance values. Additionally, environmental factors such as cloud cover and aerosol variability can introduce further uncertainties. This can result in observing different SSI values. Nevertheless, these ground-based measurements have proven to be relevant. They have shown that the ATLAS-3 spectrum [18] is inaccurate, particularly in certain wavelength bands [14,16,17], notably in the NIR and around 1600 nm. This has been confirmed by SSI observations made by the SOLar SPECtrometer (SOLSPEC) instrument on board the International Space Station (ISS) and by the implementation of the SOLAR-ISS reference solar spectrum [2].

Space-based instruments have the advantage of being able to observe the solar spectrum continuously and consistently. Over the past 30 years, numerous satellite experiments have been conducted to measure the solar spectrum from space, therefore avoiding the effects of atmospheric absorption and scattering. While prelaunch calibrations and char-

acterization procedures achieve very low uncertainties, verifying or recalibrating such instruments once in space becomes highly challenging. Studies have shown that solar spectra measured from satellites can differ significantly from each other due to instrument degradation caused by the harsh space environment [19,20] and the difficulties in accounting for changes between preflight calibration and operational conditions in space [21].

3. Calibration of the UNIS NIR Spectrometer

Preflight calibrations of the UNIS NIR spectrometer of the Uvsq-Sat NG satellite (Figure 1) are crucial for ensuring the accuracy and reliability of the SSI measurements both on the ground and in orbit. Several key spectrometer characteristics must be measured:

- Pixel characterization: Each pixel of the InGaAs linear image sensor in the UNIS NIR spectrometer has unique characteristics such as dark current, dark offset, and gain. This characterization is essential to accurately determine the incident irradiance from the digital signal output, as pixels may respond non-linearly to changes in irradiance.
- Photosensitivity and quantum efficiency: This characterization is important for accurately converting the digital signals from the UNIS linear sensor into irradiance for all wavelengths.
- Wavelength calibration: It represents a procedure that assigns a specific wavelength to each pixel of the UNIS linear sensor.
- Linearity: A calibration to verify the linearity of the signal with respect to the source intensity.
- Spectrometer bandwidth: Accurate measurement of the bandwidth, determined by the slit width and the grating's dispersion, is vital. This ensures the spectrometer's capability to resolve closely spaced spectral lines, therefore delivering the required spectral resolution data.
- Absolute response: It represents an essential characterization for ensuring the spectrometer's accuracy, reliability, and consistency of future UNIS SSI observations.
- Inverse Square Law Verification: Confirm that the intensity of light received by the spectrometer decreases inversely with the square of the distance from the light source.
- Bidirectional Reflectance Distribution Function (BRDF) and angular responses: Measurements to predict how light will be reflected or transmitted at varying angles.
- Straylight: Characterization of the stray light to ensure that the spectrometer maintains its sensitivity, dynamic range, and spectral resolution.
- Temperature response: This characterization is important to ensure accurate, stable, and reliable SSI observations of the UNIS NIR spectrometer under different thermal conditions.

Below, we present the main calibrations we have performed and the associated results.
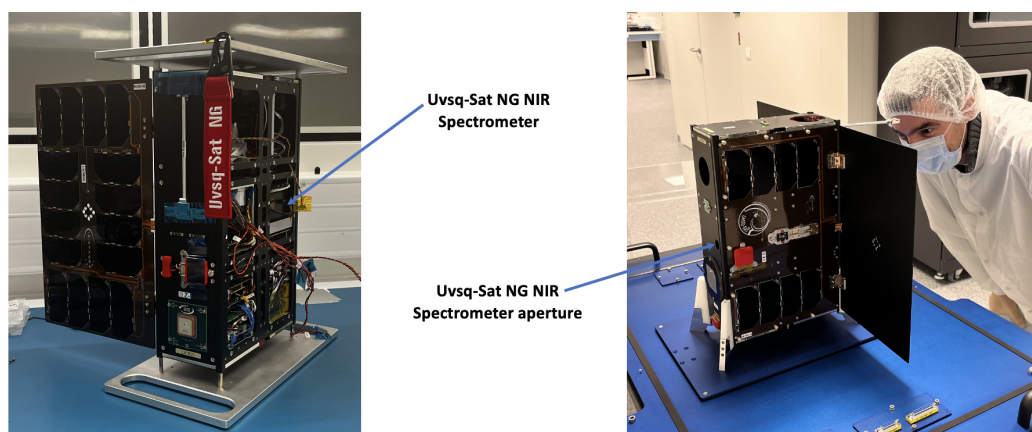

Figure 1. (**left**) Location of the Uvsq-Sat NG NIR spectrometer (UNIS) inside the satellite. (**right**) Location of the UNIS NIR spectrometer aperture on the Uvsq-Sat NG satellite.

3.1. Wavelength Calibration

Wavelength calibration of the UNIS NIR spectrometer is based on exploiting the relationship between wavelength and pixel position across the spectrometer sensor using wavelength reference standards. Typically, this involves fitting a low-order polynomial to pixel position and wavelength coordinates for a series of known peaks from a reference light source. To achieve this, we set up a test bench where a typical reference lamp with known atomic lines faces the UNIS NIR spectrometer. Figure 2 displays the various lamps utilized for this calibration. Additionally, we used a cylindrical Helium-Neon (He-Ne) Laser (Melles Griot 25-LIR-151-131). Table 1 presents the prominent lines for Hg, Xe, and Kr, as referenced in the National Institute of Standards and Technology (NIST) strong lines database (https://physics.nist.gov/PhysRefData/ASD/lines_form.html, accessed on 25 September 2024), which are relevant for the calibration of the UNIS NIR spectrometer.
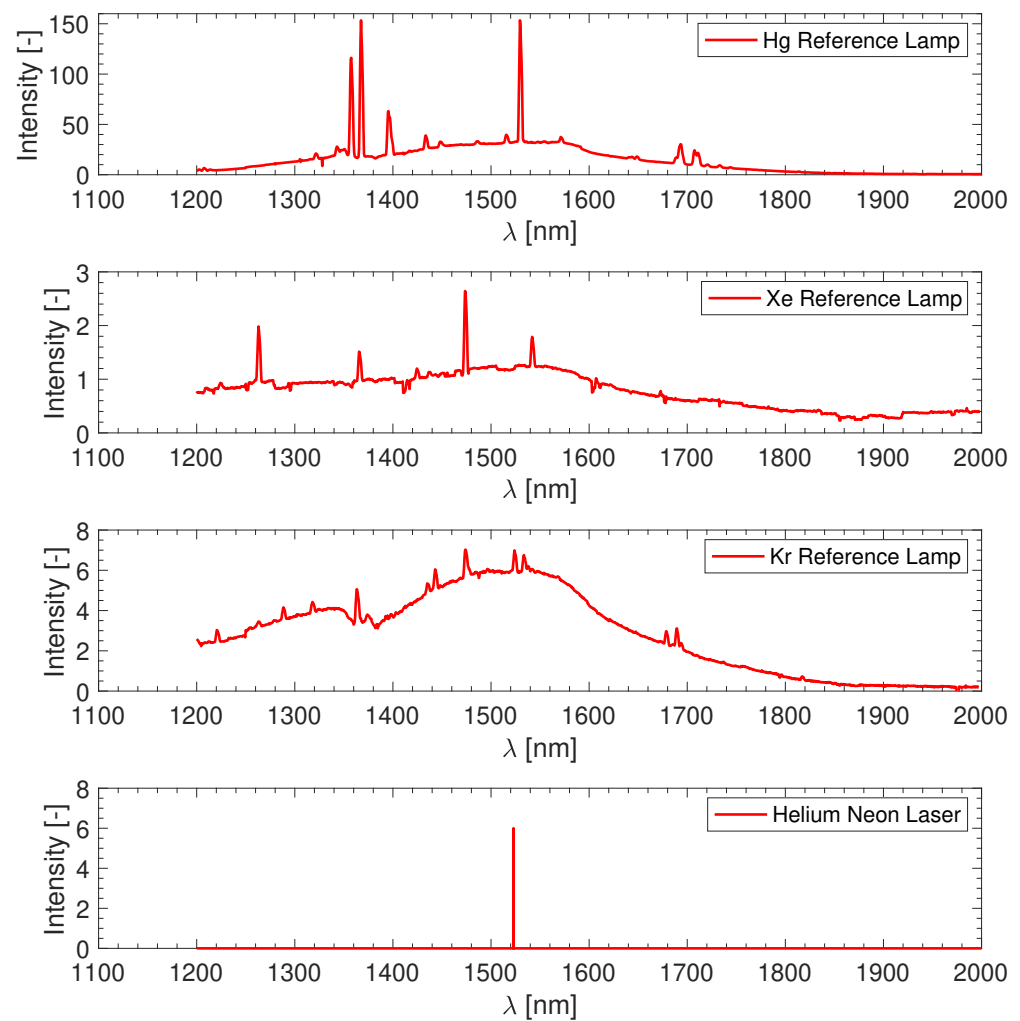

Figure 2. Spectra of the various lamps (Hg, Xe, Kr) and laser (He-Ne) used for wavelength calibration of the UNIS NIR spectrometer of the Uvsq-Sat NG space-based mission.

When observing a source of atomic emission lines with known wavelengths from Hg, Xe, or Kr lamps or a He-Ne laser, we can identify the pattern of lines and match each one to its measured pixel position. Figure 3 shows an example of a Hg lamp used as a source to identify the pixel position of the UNIS NIR spectrometer. The relationship between line wavelength and pixel position is influenced by factors such as grating geometry, groove density, focal length, pixel size, but also bandwidth. However, instead of fitting a physical model, it is practical and standard to empirically capture this relationship using a polynomial fit.

Table 1. Hg, Xe, Kr, and He-Ne strong lines with relative intensities (Rel. Int.).

Ion	λ–Air [nm]	Unc. [nm]	Rel. Int.
	1128.710	0.0400	1000
	1357.021	0.0200	200
	1367.351	0.0200	300
Hg I	1395.055	0.0200	200
	1529.582	0.0200	600
	1692.016	0.0200	1600
	1707.279	0.0200	80
	1108.524	0.0004	1900
	1174.224	0.0004	1750
	1295.644	-	2.3×10^4
	1314.671	-	1.5×10^4
Xe I	1473.238	0.0100	200
	1665.763	-	2.8×10^4
	1672.816	0.0008	5000
	1732.580	0.0009	1650
	1878.815	0.0011	860
	1286.189	0.0004	76,000
Kr I	1373.886	0.0004	310,000
	1404.566	0.0004	106,000
He-Ne	1523.071	-	-
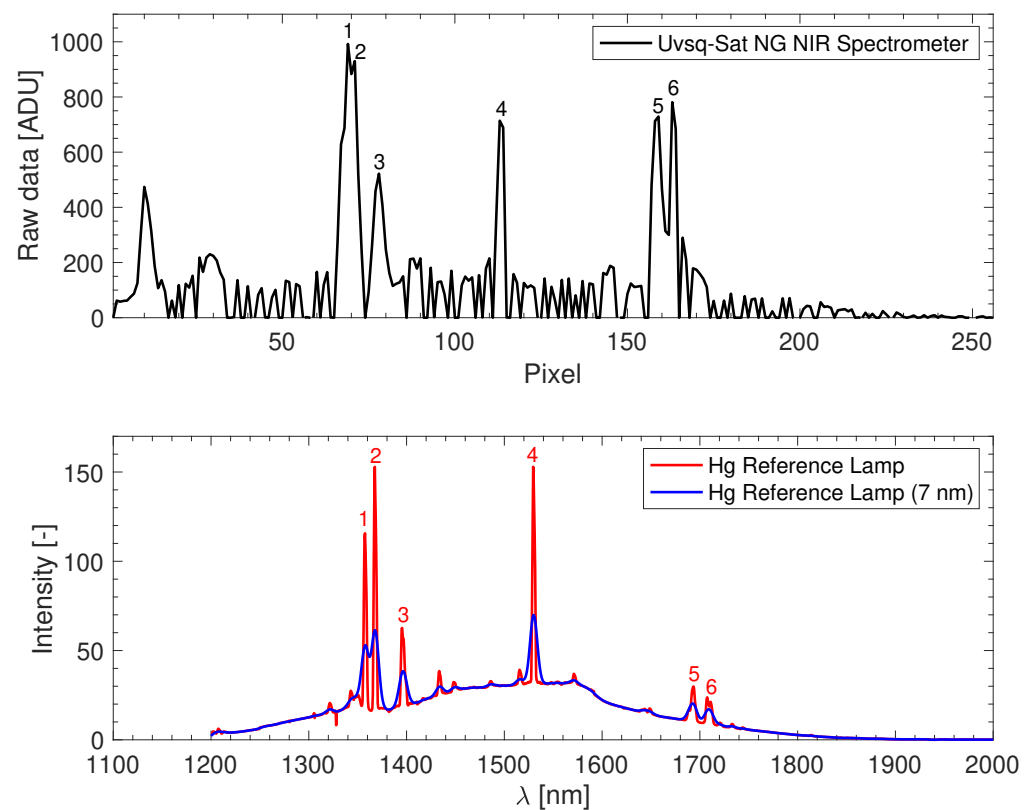
Figure 3. (**top**) Signal measured by the Uvsq-Sat NG NIR spectrometer (UNIS) when facing the Hg reference lamp. (**bottom**) The spectrum of the Hg lamp with the location of strong lines (nominal signal and signal convolved with a spectral resolution of 7 nm).

The relationship between pixel position and wavelength (Figure 4) is obtained from the calibration spectrum of various lamps and the laser. A dark spectrum was taken immediately following the Hg/Xe/Kr/He-Ne spectrum with the same exposure time, and a line list for Hg I, Xe I, and Kr I was developed for this specific spectrum, associating observed line positions with known NIST wavelengths. Some lines could not be used because, at the UNIS spectrometer's spectral resolution, they are insufficiently intense to be detected with a significant signal-to-noise ratio (SNR).
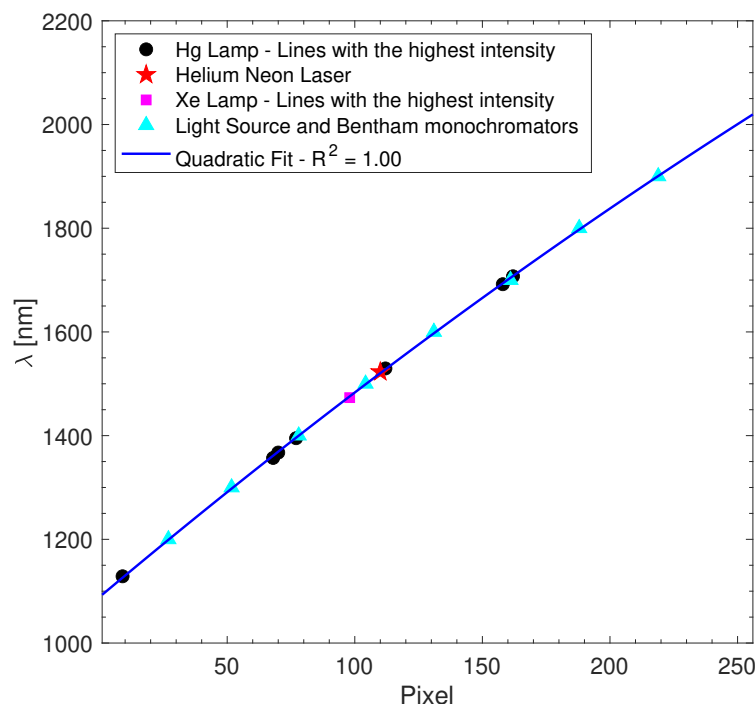
Figure 4. Pixel-wavelength relationship of the spectrometer obtained from various calibrations (lamps, laser, light source, and monochromators).

To enhance the relationship between pixel position and wavelength, we used another test bench (light source and monochromators), which also serves to determine the spectrometer's bandwidth (Section 3.3). This setup allows for identifying the positions of 8 additional wavelengths, as shown in Figure 4.

The relationship between pixel position and wavelength depends on several parameters, resulting in uncertainties. The uncertainty in determining the pixel position for the reference lamps and laser is approximately ± 0.5 nm. For the test bench with a light source and monochromators (uncertainty of about ± 0.15 nm), which uses a Gaussian fit for beams at 100 nm steps, the uncertainty is around ± 0.2 nm. For wavelengths obtained from NIST, the uncertainty is approximately ± 0.001 nm. Due to these uncertainties in pixel position determination and inherent calibration function errors, the average propagated error in the wavelength measurement is approximately 1.5 nm. Observing the Sun directly with the spectrometer offers an opportunity to refine this calibration.

3.2. Absolute Response

The bench test for absolute calibration involves precise geometric alignment of the 1000 W quartz-halogen lamp and the UNIS NIR spectrometer. The lamp must be aligned on the optical axis, which is the line perpendicular to and centered on the spectrometer. A laser is used to locate this optical axis, and the lamp is then aligned with the laser beam. The laser and lamp are mounted on an optical setup that provides several degrees of freedom, facilitating accurate alignment.

The main component of this test bench is a 1000 W quartz-halogen lamp (F-546) with a coiled-coil tungsten filament calibrated by NIST. It serves as a standard for spectral

irradiance from 1100 nm to 2000 nm. The lamp was calibrated in the NIST Facility for Automated Spectroradiometric Calibrations (FASCAL) using equipment and procedures described in [22]. The test lamp was spectrally compared to the working standards F-350, F-351, and F-355 to determine its spectral irradiance. The spectral irradiance values for this standard lamp were assigned relative to the International Temperature Scale of 1990 (ITS-90) [23]. The results of the F-546 calibration are provided in Table 2, showing the spectral irradiance (Figure 5, bottom) of the lamp and calibration uncertainties [22,24].

Table 2. Spectral irradiance (ϕ) of the F-546 lamp at a distance of 50 cm and overall uncertainty of calibration (ξ).

λ [nm]	ϕ [mW.m^{-2}.nm^{-1}]	ξ (k = 2) [%]
1100	207.45	1.11
1200	189.90	1.12
1300	170.40	1.13
1540	126.10	1.36
1600	116.40	1.42
1700	101.60	1.65
2000	67.72	2.33

The UNIS NIR spectrometer was positioned 50 cm from the F-546 reference lamp, allowing for the measurement of the signal observed by the spectrometer (Figure 5, top) and the determination of its absolute response (Figure 6) and transfer function (TF) from the precise knowledge of the F-546 calibrated flux.
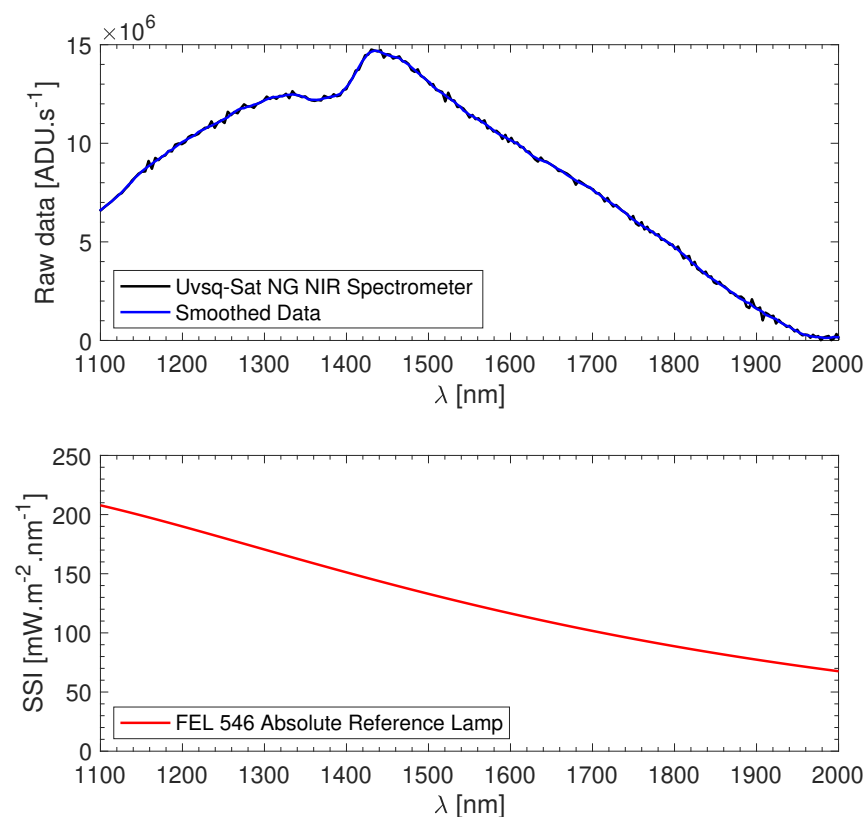

Figure 5. (**top**) Signal observed by the Uvsq-Sat NG NIR spectrometer (UNIS), with data corrected for dark current. (**bottom**) SSI of the F-546 (FEL 546) reference lamp used under standard conditions (8.2 A, distance of the device under test at 50 cm).
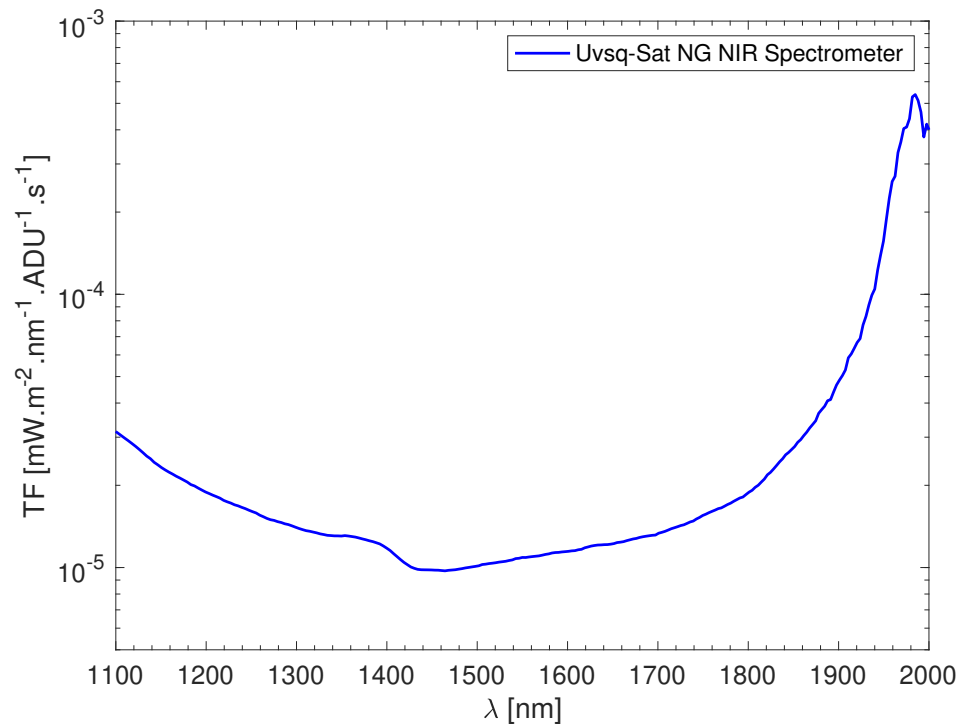
Figure 6. Absolute response (TF) of the Uvsq-Sat NG NIR spectrometer (UNIS) from 1100 to 2000 nm.

3.3. Bandwidth and Slit Functions

The bandwidth of the spectrometer was initially evaluated using a laser at a wavelength of 1523 nm. Figure 7 shows the full width at half maximum (FWHM) of the slit function of the UNIS NIR spectrometer for this particular wavelength.
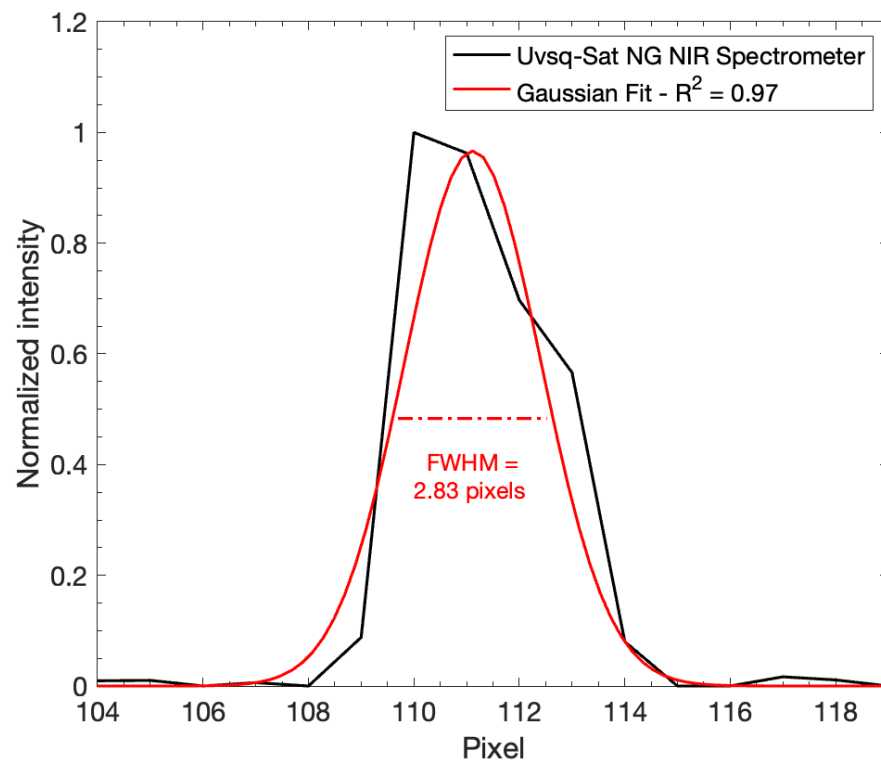

Figure 7. FWHM of the slit function of the Uq-Sat NG NIR spectrometer (UNIS) at 1523 nm, determined using a laser.

To determine the slit functions of the UNIS spectrometer and its FWHM across the entire range of wavelengths, we set up a new test bench (TB1). At the top of the setup, a stable light source, typically a 1000 W Quartz Tungsten-Halogen (QTH) lamp (LSB127 from L.O.T Oriel), is mounted in a lamp housing (LSH601 from L.O.T Oriel) and fitted with a condenser (LSN610 from L.O.T Oriel) to focus the light onto the first monochromator (Bentham TM300). The lamp provides excellent radiance stability (0.1%), surpassing the 0.5% stability reported in previous studies [25]. The focused light then enters the system through an entrance slit, which controls the amount of light entering the monochromator. Inside the first monochromator, mirrors direct the light beam toward a gratings turret. The gratings turret contains diffraction gratings that disperse the light into its component wavelengths. The dispersed light passes through an intermediate slit, which further refines the light beam. A filter wheel on the first monochromator ensures constant operation at the first order of diffraction. The light then enters the second monochromator (Bentham TM300), where it undergoes a similar process of reflection by mirrors and dispersion by a second gratings turret. This double monochromator setup enhances the spectral purity of the output light by significantly reducing stray light and unwanted higher-order diffraction effects. After passing through the second monochromator, the refined light exits through an exit slit, providing a stable and tunable monochromatic light beam from 1100 to 2000 nm. This exit slit ensures that only the desired wavelength band reaches the next stage of the setup. The light exiting the second monochromator is captured by an optical fiber (FOP-NUVIR from Bentham). The UNIS spectrometer receives the transmitted light through this optical fiber for accurate calibration. It measures the light intensity and wavelength, providing data for the calibration and determination of the spectrometer's bandwidth.

A beam splitter placed after the optical fiber can also be used to divide the signal between the UNIS NIR spectrometer and a Ge NIR detector (Newport Inc. 71653) calibrated at Physikalisch-Technische Bundesanstalt (PTB). In this setup, the calibrated NIR detector is not used for absolute calibration but rather to quantify the monochromatic optical power illuminating the UNIS NIR spectrometer across all tested wavelengths, therefore enabling normalization.

The use of two monochromators (double monochromators) in series significantly improves the spectral resolution and stray light rejection compared to a single monochromator. This results in a tunable monochromatic flux with high spectral purity. Additionally, the setup allows for the use of neutral density (ND) filters to adjust the radiance and achieve various levels of attenuation. This capability ensures that the spectrometer can be tested under different illumination conditions. The double monochromator setup, combined with precise optical alignment using lenses, slits, and optical fibers, ensures highly accurate calibration of the spectrometer's wavelength scale and bandwidth determination. By employing this detailed setup, the UNIS NIR spectrometer can be precisely calibrated, ensuring reliable and accurate spectral measurements essential for the Uvsq-Sat NG space-based mission.

Using this test bench, we determined the slit functions of the spectrometer and the FWHM between 1100 and 2000 nm. The initial setup, which involved the use of an optical fiber, was not successful because there was insufficient signal at the fiber's output to accurately characterize the spectrometer's bandwidth. Therefore, we positioned the spectrometer directly at the exit slit of the double monochromator. Figure 8 shows the results obtained. The determination of the UNIS bandwidth is challenging because, even in this configuration, the flux at the exit of the double monochromator is occasionally insufficient to accurately resolve the spectrometer's bandwidth across all wavelengths.

To improve this test and increase the accuracy of the Bandwidth Calibration, a second spectral test bench (TB2) was developed. TB2 is designed to measure the slit functions of the UNIS NIR spectrometer over the 1100 to 2000 nm range, with an accuracy better than 1 nm. To achieve this, the second bench test primarily consists of a Xenon lamp and a monochromator (Horiba iHR320) equipped with a grating blazed at 600 grooves/mm. The Xenon lamp's flux is focused on the monochromator's entrance slit to minimize flux losses between the lamp and the spectrometer. At the monochromator slit exit, the flux

is collimated towards a beam splitter, which divides the optical path into two separate paths: one directed towards a reference InGaAs detector, and the other towards the UNIS spectrometer. The collimated flux at the monochromator slit exit minimizes flux losses, given the instrument's 0.15° field of view. This setup maximizes the signal received by the UNIS NIR spectrometer. However, without the use of an optical fiber, it requires greater alignment precision. These efforts are ongoing.
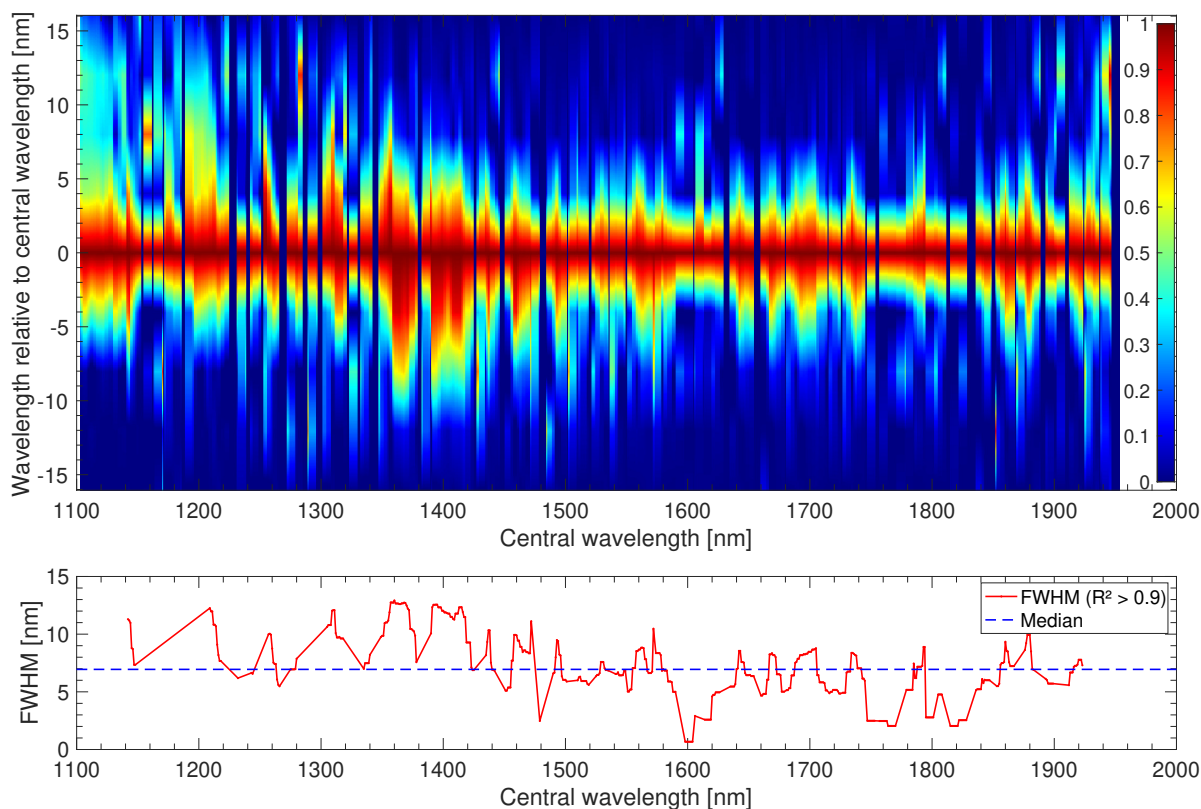

Figure 8. (**top**) Distribution of relative spectral responses (slit functions) of the Uvsq-Sat NG NIR spectrometer (UNIS). (**bottom**) FWHM values of the slit functions of the spectrometer.

3.4. Temperature

The temperature characterization of the UNIS NIR spectrometer is important to ensure accurate, stable, and reliable SSI observations across various thermal conditions. Understanding how temperature affects the spectrometer's readings allows for the implementation of appropriate corrections, ensuring the integrity of the data collected during the mission. Figure 9 shows an example of the temperature response of the UNIS NIR spectrometer at a wavelength of 1600 nm. It clearly demonstrates that the lower the temperature of the spectrometer, the lower the noise level. This test highlights the importance of operating the spectrometer at a lower temperature, with an optimal operating point below 5 °C, to minimize dark current.
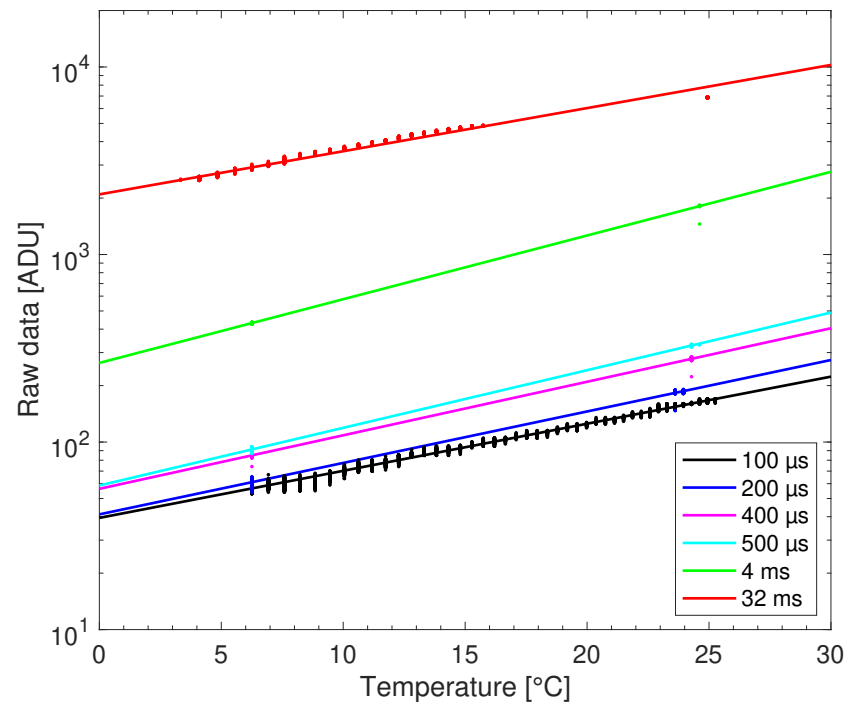
Figure 9. Temperature response (dark current) of the Uvsq-Sat NG NIR spectrometer (UNIS) during a test in a climatic chamber (26 April 2024). The raw data (ADU) is plotted against temperature (°C) for various exposure times.

4. Determining Extraterrestrial Solar Spectrum Using the Langley-Plot Technique

The Langley-plot technique [26] is a method used for determining the extraterrestrial solar spectral irradiance ($I_{0,\lambda}$) by measuring the direct SSI ($I_{obs,\lambda}$) at the Earth's surface under various air masses. This method involves extrapolating surface measurements to AirMass 0 (AM0), which represents SSI at TOA. Below is the methodology applied in our observations, focusing on the spectral range from 1100 nm to 2000 nm and conducted under clear sky conditions to minimize atmospheric interference.

To assess the uncertainties in the UNIS NIR spectrometer's on-site SSI observations using the Langley-plot method, we used the approach implemented during the PYR-ILIOS campaign at Mauna Loa Observatory [17].

4.1. Methodology

Direct solar spectral irradiance ($I_{obs,\lambda}$) is measured at the Earth's surface over a range of air masses, typically during sunrise or sunset when the solar zenith angle changes significantly. Measurements are taken under clear sky conditions to minimize the effects of clouds.

The AirMass (AM) is calculated using the adopted model proposed by Kasten and Young [27], which is given by Equation (1), i.e.,

$$\text{AM} \simeq \frac{1}{\cos(z) + 0.50572 \times (96.07995 - z)^{-1.6364}} \tag{1}$$

where z is the solar zenith angle, which can also be obtained using the National Oceanic and Atmospheric Administration (NOAA) Solar Geometry Calculator (https://gml.noaa.gov/grad/antuv/SolarCalc.jsp?mu=on&sza=on&el=on&az=on, accessed on 25 September 2024).

According to the Beer-Lambert law, $I_{obs,\lambda}$ is related to $I_{0,\lambda}$ by Equation (2), i.e.,

$$I_{obs,\lambda} = I_{0,\lambda} \times \exp(-\text{AM} \times \tau(\lambda)) \times \left(\frac{1\,\text{au}}{d_z}\right)^2 \qquad (2)$$

where $\tau(\lambda)$ is the total optical depth, and d_z is the distance between Earth and the Sun. The astronomical unit (1 au) is equal to 149,597,870.7 km.

Taking the natural logarithm on both sides of Equation (2), we obtain:

$$\ln(I_{obs,\lambda}) = \ln\left(I_{0,\lambda} \times \left(\frac{1\,\text{au}}{d_z}\right)^2\right) - \text{AM} \times \tau(\lambda) \qquad (3)$$

By plotting $\ln(I_{obs,\lambda})$ or log10 against AM, a Langley-plot is created. A linear regression is performed on this plot to find the best-fit line. The slope of this line gives the total optical depth $\tau(\lambda)$, and the y-intercept gives $\ln(I_{0,\lambda})$. Extrapolating the best-fit line to AM = 0 allows the determination of the extraterrestrial SSI ($I_{0,\lambda}$).

Using the UNIS NIR spectrometer, we can acquire a large volume of data with an acquisition time of a few hundred microseconds to observe the center of the solar disk ($\mu = 1$). Consequently, we have developed two methods to process these data.

Method M1 (Langley-plot Extrapolation with Interval Refinement) involves calculating the SSI for each wavelength within the 1100–2000 nm range. The process begins with initializing an array to store the extrapolated irradiance values. For each wavelength, the measured spectral data are selected and corrected for dark current, temperature, filter transmission, and other factors. Next, the corresponding AM values are calculated using interpolation. The logarithm of the filtered irradiance values is computed to linearize the data. The AirMass range is divided into a specified number of intervals (20 in this case), and arrays are initialized to store the maximum logarithmic irradiance and average AirMass for each interval. For each AirMass interval, the maximum logarithmic irradiance is identified, and the average AirMass for that interval is calculated. An initial linear regression is performed on the maximum logarithmic irradiance values against the average AirMass values to find the initial fit line. Data points below the initial regression line are eliminated, and new maximum values for each interval are determined from the refined data. A second linear regression is performed on the refined set of maximum values and average AirMass values. The fit line is then extrapolated to an AirMass of zero to determine the extrapolated irradiance, representing the SSI at TOA. Finally, the extrapolated irradiance value for each wavelength is stored in the output array. This method leverages the Langley-plot technique, which involves plotting the logarithm of observed irradiance against AM to determine the extraterrestrial solar irradiance ($I_{0,\lambda}$). The linear regression on this plot provides the SSI by extrapolating to AM0, assuming a consistent optical depth throughout the measurement period.

Method M2 (Iterative Langley-plot Refinement) involves calculating the SSI using an iterative approach to refine the linear regression and improve the accuracy of the extrapolation to AM0. For each wavelength, the measured spectral data are selected and corrected for dark current, temperature, filter transmission, and other factors. Next, the corresponding AM and temperature values are interpolated for the selected data points. The logarithm of the filtered irradiance values is computed to linearize the data. An initial linear regression is performed on the logarithmic irradiance values against AM values to find the slope and intercept. The fit line is then extrapolated to AM0 to determine the initial SSI. To refine the data, an iterative process is used. Variables for the iterative process, including the R-squared value, tolerance, maximum iterations, and a sigma threshold for residuals, are initialized. The iteration begins by performing linear regression, calculating predicted values and residuals, and computing the R-squared value to assess the fit quality. If the R-squared value meets the tolerance, the iteration stops. Otherwise, data points within a specified sigma threshold are filtered. The AM and logarithmic irradiance data are updated with the refined set of points, and the iteration counter is incremented. This

process repeats until the tolerance is met or the maximum number of iterations is reached. Finally, the extrapolated irradiance at AM0 is determined using the final intercept from the refined regression, representing the SSI. The extrapolated irradiance value for each wavelength is stored in the output array. This iterative refinement ensures a more robust determination of the SSI by improving the linear regression fit, therefore providing a more accurate extrapolation to AM0.

4.2. Consideration of Atmospheric Effects

Several atmospheric components affect the measured solar spectral irradiance. Determining them would provide a good understanding of the impact of the different components of the total optical depth.

4.2.1. Rayleigh Scattering

Rayleigh scattering, caused by the scattering of light by air molecules, is significant in the ultraviolet and visible regions but decreases with increasing wavelength. For wavelengths between 1100 nm and 2000 nm, the Rayleigh scattering optical depth (τ_R) can be calculated using the formula provided by [28], as in Equations (4)–(6), i.e.,

$$\tau_R(\lambda) = \frac{\sigma_r(\lambda) \times N_A \times P_0}{M_{\text{air}} \times g} \simeq 0.002152 \cdot 10^{28} \times \sigma_r(\lambda) \times (1 + \delta) \tag{4}$$

with

$$\sigma_r(\lambda) \simeq 10^{-28} \times \left(1.0455996 - 341.29061\lambda^{-2} - 0.9023085\lambda^2 \right)$$
$$\times \left(1 + 0.0027059889\lambda^{-2} - 85.968563\lambda^2 \right)^{-1} \tag{5}$$

$$\text{and } \delta = 0.54 \times \left(\frac{[\text{CO}_2]}{385\text{ppm}} - 1 \right) \tag{6}$$

where λ is the wavelength in μm, $\sigma_r(\lambda)$ is the molecular scattering cross-section (cm^2 per molecule), N_A is Avogadro's number, P_0 is the atmospheric pressure at sea level, M_{air} is the molar mass of air, and g is the acceleration due to gravity. δ represents the correction factor for the current CO_2 concentration (∼425 ppm).

4.2.2. Ozone Absorption

Ozone (O_3) absorbs light primarily in the ultraviolet and visible regions. For the infrared region (1100 nm to 2000 nm), ozone absorption is less significant but still accounted for using known ozone absorption cross-sections and local ozone concentration profiles to calculate the O_3 optical depth (τ_{O_3}).

4.2.3. Mie Scattering and Aerosols

When the size of particles ranges between 0.1 and 10 times the wavelength of solar radiation, Rayleigh scattering no longer occurs, giving way to Mie scattering, also known as non-molecular or aerosol particle scattering. Mie scattering is much less selective than Rayleigh scattering. Common causes of Mie scattering include dust, pollen, smoke, microscopic water droplets that form clouds, and volcanic ash. These aerosols contribute to the attenuation of light through both scattering and absorption processes. The aerosol optical depth, τ_a (Equation (7)), quantifies the extent of light attenuation due to aerosols. It can be determined using measurements from the UNIS NIR spectrometer or estimated through empirical models.

$$\tau_a(\lambda) = \tau_a(\lambda_0) \left(\frac{\lambda_0}{\lambda} \right)^\alpha \tag{7}$$

where $\tau_a(\lambda_0)$ is the aerosol optical depth at a reference wavelength (λ_0), and α is the Ångström exponent. For clean maritime air, $\tau_a(500 \text{ nm})$ is close to 0.10 and $\alpha \simeq 1.0$. For high pollution, $\tau_a(500 \text{ nm})$ is close to 0.35 and $\alpha \simeq 1.5$.

4.2.4. Other Gases

Other gases such as water vapor (H_2O), carbon dioxide (CO_2), and methane (CH_4) absorb light in the infrared region. Their contributions can be estimated using known concentration profiles and absorption cross-sections.

4.3. Comprehensive Calculation of Optical Depth

The total optical depth (τ) at each wavelength is obtained as in Equation (8), i.e.,

$$\tau(\lambda) = \tau_R(\lambda) + \tau_{O_3}(\lambda) + \tau_a(\lambda) + \tau_g(\lambda) \tag{8}$$

where $\tau_g(\lambda)$ represents the optical depth due to other gases.

The Langley-plot, derived from UNIS NIR observations, provides the total optical depth as the slope of the linear regression, allowing for an estimation of aerosols.

Different quantities observed with the UNIS NIR spectrometer, including aerosols, can also be obtained by inverting NIR spectra to determine X_{CO_2}, X_{CH_4}, X_{O_2}, X_{H_2O}, X_{Rayl}, and X_{aer} using the Levenberg-Marquardt method [1]. This approach, which will be discussed in another manuscript, aims to quantify each parameter to estimate $I_{0,\lambda}$.

4.4. Conditions for Accurate Measurements Using the Langley Technique

To perform accurate measurements using the Langley technique, several conditions must be met to minimize errors and obtain reliable results. First, clear skies are essential. Measurements should be conducted during clear weather, without clouds, haze, or fog, to avoid additional absorption or scattering of light that could skew the results. Second, atmospheric stability is crucial throughout the measurement period. Rapid changes in atmospheric conditions, such as variations in aerosol or water vapor content, can introduce errors. Third, a wide range of zenith angles is necessary. Measurements should cover a broad range of zenith angles, ideally from sunrise to sunset, to ensure comprehensive coverage of AM. This allows for a precise linear regression for the Langley-plot technique. Fourth, precise laboratory calibration of the spectrometer is required (Section 3). Fifth, accurate calculation of AM is essential, which should be precisely calculated based on the zenith angle and the altitude of the site. Sixth, aerosol homogeneity is important. The aerosol distribution should be homogeneous during the measurement period to avoid local variations in optical extinction that could affect the results. Seventh, the absence of transient pollution is necessary. Measurements should be conducted away from local pollution sources (such as industrial areas or forest fires) that can cause transient variations in optical extinction. Eighth, documentation of weather conditions is crucial. Meteorological conditions should be well-documented to explain or correct any anomalies observed in the data.

By adhering to these conditions, precise and reliable measurements of SSI can be obtained, as well as an accurate determination of atmospheric parameters such as the optical thickness of aerosols.

5. Experiment Results and Discussion

The UNIS NIR spectrometer underwent calibration in the laboratory during the first quarter of 2024, adhering to the procedures detailed in Section 3. Following these calibrations, we conducted a test campaign to perform direct measurements of the Sun. These measurements were aimed at verifying the absolute calibration of the spectrometer conducted in the laboratory and providing an extraterrestrial solar spectrum using the Langley-plot technique. The test campaign was conducted on 9 May 2024 at the Pommier site in Charente-Maritime (45.54°N, 0.83°W), situated at an altitude of 50 m above sea level. We chose this site because it is in a region of France that frequently enjoys sunny weather and is relatively close to our laboratory. Additionally, the absence of industrial sites in this location results in minimal pollution. These factors make it an optimal location for our testing campaign, even though it is at a low altitude. Studies have shown that sites at low

and medium altitudes, distant from natural or anthropogenic pollution sources, can achieve sufficient atmospheric optical stability to obtain calibration coefficients [29,30]. Therefore, given appropriate topographic conditions in lowlands, the Langley-plot technique can be successfully used.

We simultaneously observed the Sun with the UNIS NIR spectrometer and an H-alpha telescope (656.281 nm) to capture images of the Sun. Figure 10 shows an example of a solar image obtained with our telescope during this test campaign. On 9 May 2024, more than 350,000 measurements were taken with the UNIS NIR spectrometer between 11:00 UTC and 18:00 UTC. During these observations, the AirMass varied from approximately 1.1 to 4.5 (Figure 11, left). Meanwhile, the instrument's temperature ranged from a minimum of 22.4 °C to a maximum of 27.4 °C (Figure 11, right).

9 May 2024 − 11H13 TU
L0 = 320.68°
B0 = -3.26°
P = 337.74°

Parallactic angle: 16.9°
1.0096 AU
31' 41''

Pommier (17), France
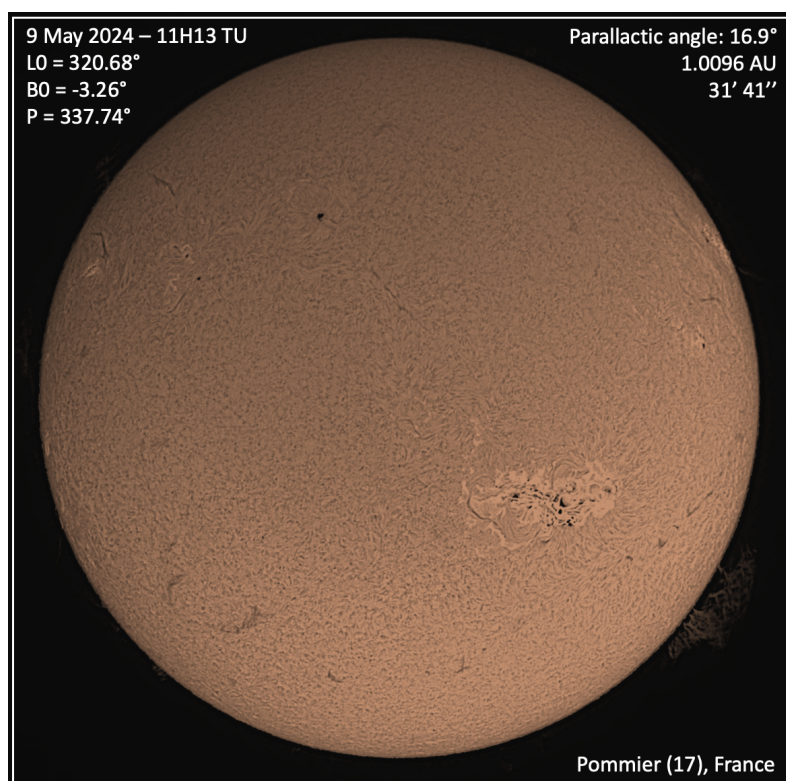
Figure 10. Image of the Sun taken in H-alpha (656.28 nm) with our telescope during the test campaign of the spectrometer. This period of observations was marked by intense solar activity characterized by powerful solar storms, extreme solar flares, and geomagnetic storm components.

Figure 12 (top) illustrates data acquired by the UNIS NIR spectrometer. Figure 12 (bottom) displays the SSI measured at two different air masses (AM 1.17 in red and AM 1.63 in blue), showing the variation in SSI across the wavelength range. These are calibrated data (physical values) obtained from the characterizations presented in Section 3. For each Frame Number, and there are more than 350,000, we have a solar spectrum observed at ground level as a function of wavelength and a given AirMass. Around 1380 nm, we should observe SSI (AM 1.17 and AM 1.63) close to zero because we are within a water vapor absorption band. It appears that the absolute response (Figure 6) could not be optimal in this wavelength range.
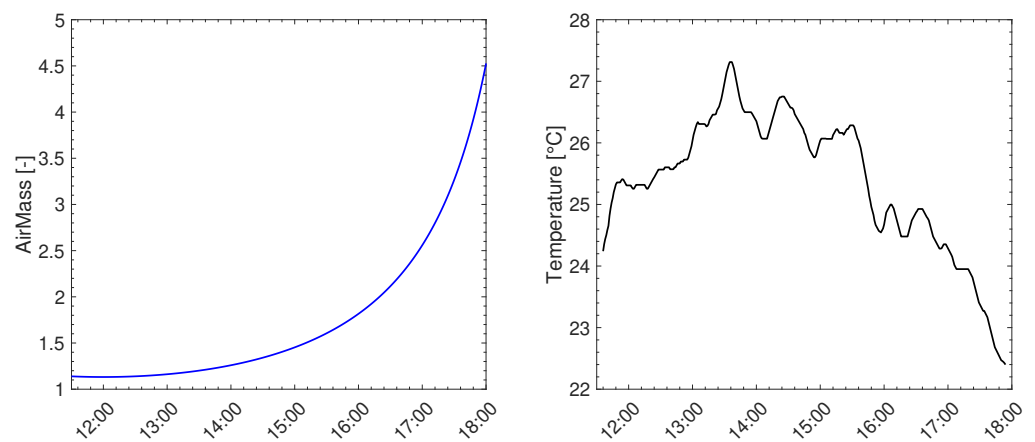
Figure 11. (**left**) Evolution of AirMass from 11:00 UTC to 18:00 UTC on 9 May 2024, at the Pommier site (Charente-Maritime). (**right**) Temperature variation during the observations.

Outside the absorption bands (notably those of water vapor), we can obtain the SSI extrapolated to the TOA using the Langley-plot technique for all measurements. The uncertainty in the extrapolation is accounted for in the error budget of the measurement. As explained in Section 4, we used two methods for determining the extraterrestrial solar spectrum within atmospheric windows.
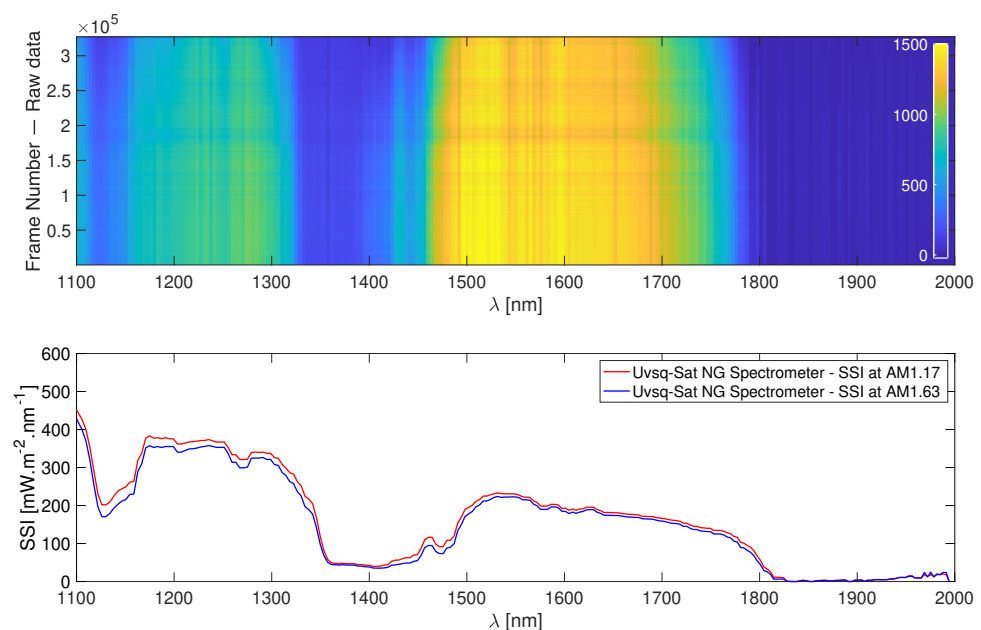
Figure 12. (**top**) Raw data intensities acquired by the Uvsq-Sat NG NIR spectrometer (UNIS) over time (Frame Number of the measurements). (**bottom**) SSI was measured by the spectrometer at air masses of 1.17 (red line) and 1.63 (blue line).

Figure A2 shows the SSI results obtained using Method 1 (Langley-plot Extrapolation with Interval Refinement), while Figure A3 shows the results obtained using Method 2 (Iterative Langley-plot Refinement). With Method 2, there is a more stringent selection of data, and the extrapolation to AM0 yields values that are slightly closer to the targeted SSI at TOA. However, Method 1 relies on a larger number of points to estimate the SSI at TOA. Nevertheless, the results between the two methods remain very close, as shown in Figures A2 and A3 (for a given example with four selected wavelengths).

Figure 13 shows the solar spectrum (outside the absorption bands) obtained with the UNIS NIR spectrometer using the two implemented methods. In the water vapor

absorption bands, the modified Langley-plot technique [31] can be used to provide SSI values in these bands.
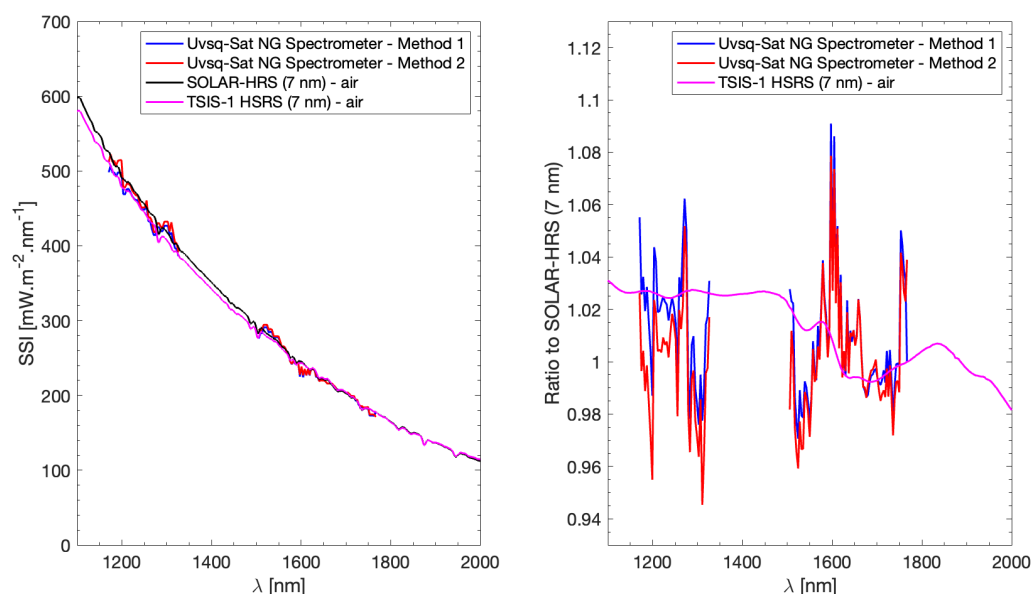
Figure 13. (**left**) Solar spectrum obtained with the Uvsq-Sat NG NIR spectrometer (UNIS) for the two methods implemented. SOLAR-HRS and TSIS-1 HSRS solar spectra are shown for comparison within a wavelength range between 1100 and 2000 nm. (**right**) The ratio of the different spectra convolved to 7 nm compared to the spectrum obtained with the UNIS NIR spectrometer.

For comparison, the SOLAR-HRS and TSIS-1 HSRS solar spectra are also displayed within the wavelength range of 1100 to 2000 nm. The spectra are consistent and highlight the quality of the observations obtained with the UNIS NIR spectrometer of the Uvsq-Sat NG mission. In particular, we focused on the SSI values recorded by the UNIS NIR spectrometer at 1600 nm. Our results are consistent with the SOLAR-HRS and TSIS-1 HSRS solar spectra, providing further evidence that ATLAS-3 is not accurate in the NIR. This aligns with the controversy that emerged in 2016, where discrepancies were noted between the ATLAS-3 composite and more recent SSI measurements in the NIR spectral region. Data from SCanning Imaging Absorption spectroMeter for Atmospheric CHartographY (SCIA-MACHY) [32], Continuum Absorption in the Visible and Infrared and its Atmospheric Relevance (CAVIAR) [13], IRSPERAD [14], PYR-ILIOS [17], SOLAR2 spectrum from SOL-SPEC/ISS [33], and the Spectral Irradiance Monitor (SIM) instrument [34] on board the Solar Radiation and Climate Experiment (SORCE) indicate that above approximately 1600 nm, SSI values are about 8% lower than those reported by ATLAS-3.

In 2018, two reference solar spectra [2,35] obtained from space-based instruments confirmed that ATLAS-3 overestimated the values above approximately 1600 nm, while ground-based observations could underestimate SSI at 1600 nm. Observations at 1600 nm are particularly valuable as this wavelength probes the deeper layers of the photosphere, where the solar atmosphere's opacity is minimal [36]. The photosphere, which extends from the visible surface to about 500 km above it, exhibits temperatures ranging from 6400 K at the bottom to 4000 K at the top. Therefore, observations at 1600 nm also allow for the measurement of the brightness temperature, reaching values close to 6400 K (Figure A4). Additionally, we are interested in observing the SSI at 1282 nm for an in-orbit calibration of the UNIS NIR spectrometer. This wavelength corresponds to the Paschen Beta line, which is produced when an electron transitions from the fourth energy level to the third energy level of a hydrogen atom. It provides valuable information about the conditions in the chromosphere, the outermost layer of the Sun, which extends from approximately 500 km above the solar surface (temperature of 4000 K) to about 2100 km (temperature up

to 8000 K). However, it cannot normally be seen because it emits relatively little light in comparison to the layer beneath it. It is only brighter than the underlying layers in a few wavelengths, such as in the NIR spectrum), such as temperature and density.

6. Conclusions

In this study, we presented the comprehensive calibration process and ground-based measurements conducted with the Uvsq-Sat NG NIR spectrometer (UNIS).

Our ground-based measurements at the Pommier site in May 2024 provided an opportunity to verify the absolute calibration of the UNIS NIR spectrometer under real conditions and to determine the solar spectrum at TOA based on the Langley-plot technique. The solar spectrum obtained with the UNIS NIR spectrometer was consistent with the SOLAR-HRS and TSIS-1 HSRS solar spectra, further validating the accuracy of our measurements. Notably, our observations at 1600 nm confirmed that the ATLAS-3 measurements were overestimated above this wavelength, aligning with recent findings from space-based instruments. The results obtained were excellent, demonstrating the reliability of our calibration process. These findings underscore the significance of the UNIS NIR spectrometer for both solar spectral observations and greenhouse gas measurements. The high precision and reliability of the instrument establish a solid foundation for future orbital data collection and analysis. In orbit, we aim to replicate these observations to obtain a direct solar spectrum at TOA and compare it with the results obtained during the May 2024 campaign. We are also aiming to establish a geophysical station in Grasse (France) to simultaneously measure the solar spectrum, greenhouse gases, and aerosols from the ground. This would provide measurements of interest to compare with Uvsq-Sat NG satellite when it passes over Grasse—also aiding in the Uvsq-Sat NG calibration efforts in orbit.

Appendix A. Optical Design of the Uvsq-Sat NG Spectrometer
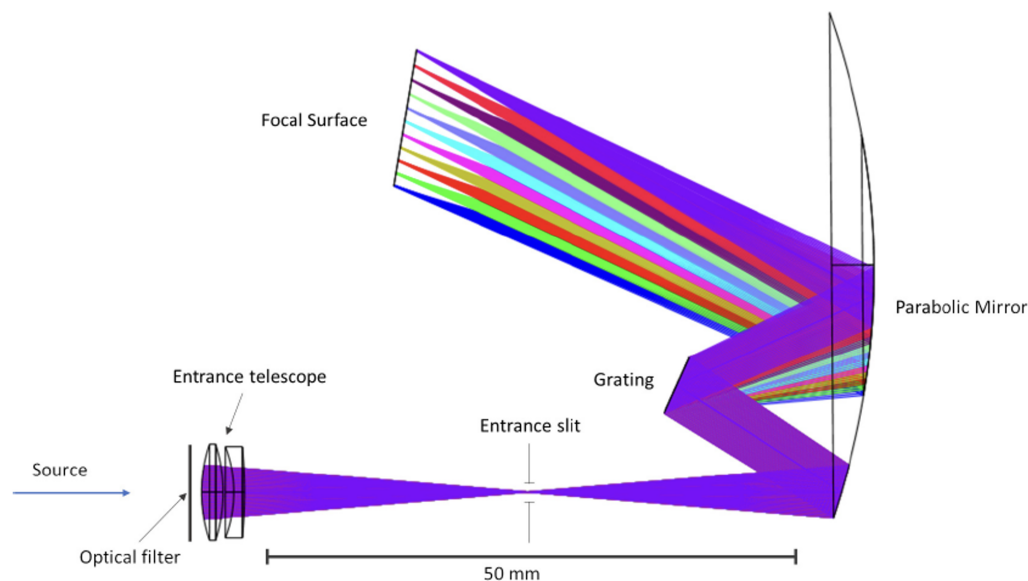

Figure A1. Optical layout of the Uvsq-Sat NG NIR spectrometer (UNIS). UNIS is a miniaturized spectrometer with an aperture of 15 mm, a spectral range from 1100 to 2000 nm, a spectral resolution of 7 nm, and a field of view of 0.15°.

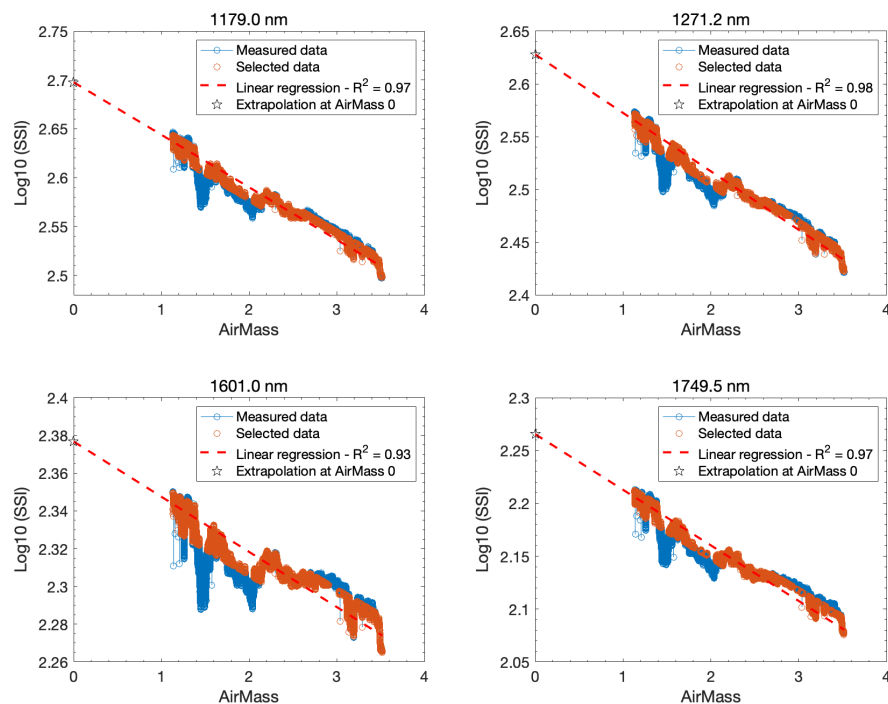## Appendix B. Observations Made with the Uvsq-Sat NG Spectrometer

Figure A2. Measured irradiance and corresponding Langley-plot fits for four wavelengths (1179.0, 1271.2, 1601.0, and 1749.5 nm) observed by the Uvsq-Sat NG NIR spectrometer (UNIS) on 9 May 2024, based on the use of Method 1.

Figure A3. Measured irradiance and corresponding Langley-plot fits for four wavelengths (1179.0, 1271.2, 1601.0, and 1749.5 nm) observed by the Uvsq-Sat NG NIR spectrometer (UNIS) on 9 May 2024, based on the use of Method 2.
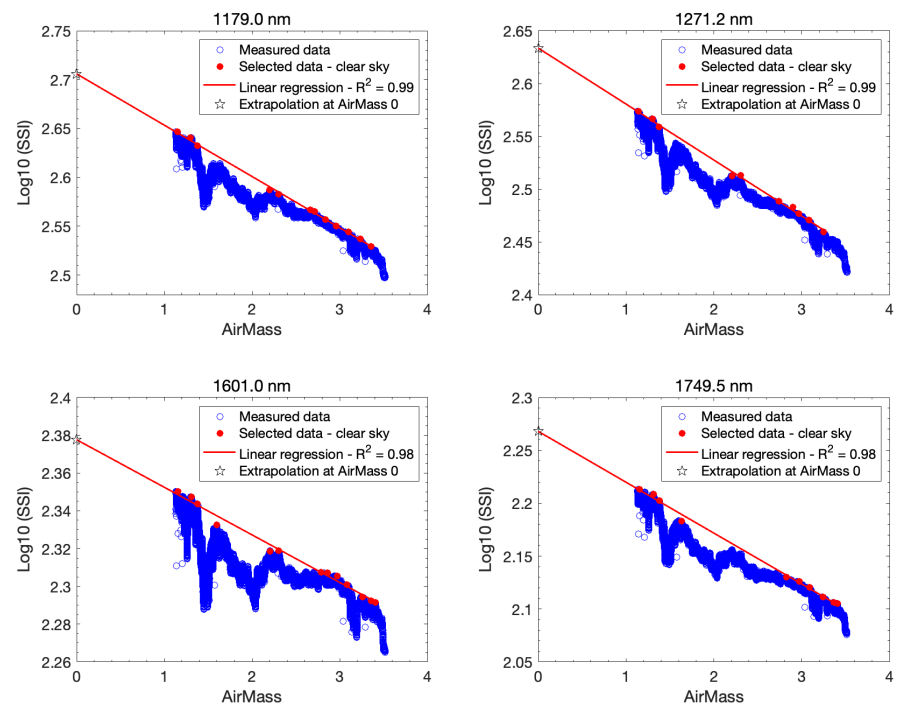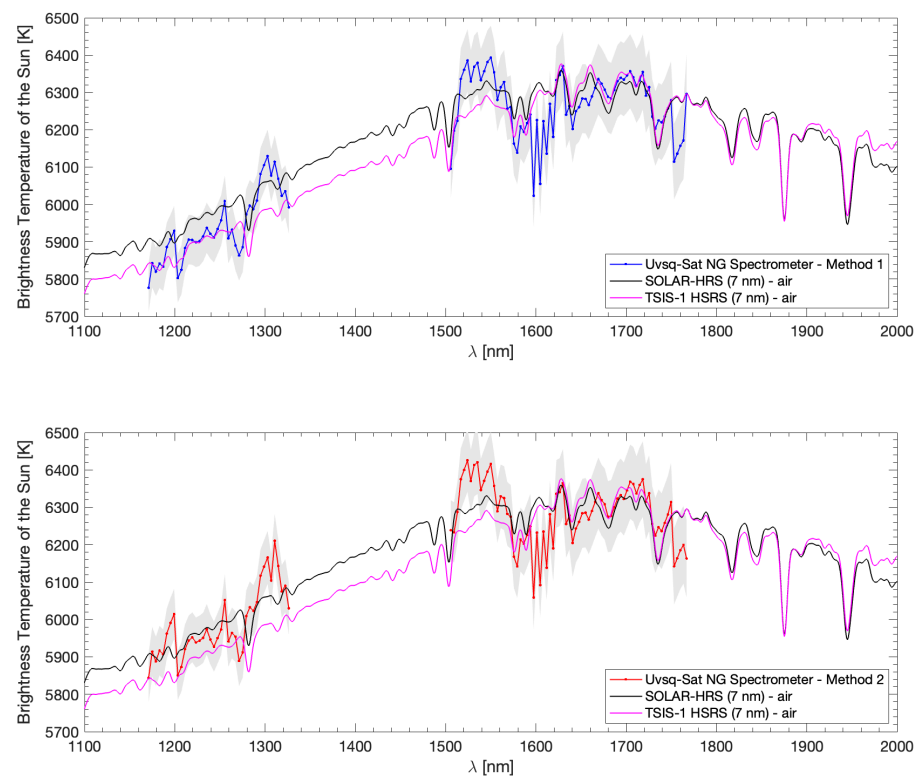

Figure A4. Brightness temperature of the Sun obtained from the Uvsq-Sat NG NIR spectrometer (UNIS) in the wavelength bands where the Langley-plot technique is applicable. The brightness temperatures from HRS and TSIS are also shown for comparison.

References

1. Meftah, M.; Clavier, C.; Sarkissian, A.; Hauchecorne, A.; Bekki, S.; Lefèvre, F.; Galopeau, P.; Dahoo, P.R.; Pazmino, A.; Vieau, A.J.; et al. Uvsq-Sat NG, a New CubeSat Pathfinder for Monitoring Earth Outgoing Energy and Greenhouse Gases. *Remote Sens.* **2023**, *15*, 4876. [CrossRef]
2. Meftah, M.; Damé, L.; Bolsée, D.; Hauchecorne, A.; Pereira, N.; Sluse, D.; Cessateur, G.; Irbah, A.; Bureau, J.; Weber, M.; et al. SOLAR-ISS: A new reference spectrum based on SOLAR/SOLSPEC observations. *Astron. Astrophys.* **2018**, *611*, A1. [CrossRef]
3. Coddington, O.M.; Richard, E.C.; Harber, D.; Pilewskie, P.; Woods, T.N.; Chance, K.; Liu, X.; Sun, K. The TSIS-1 Hybrid Solar Reference Spectrum. *Geophys. Res. Lett.* **2021**, *48*, e91709. [CrossRef] [PubMed]
4. Meftah, M.; Sarkissian, A.; Keckhut, P.; Hauchecorne, A. The SOLAR-HRS New High-Resolution Solar Spectra for Disk-Integrated, Disk-Center, and Intermediate Cases. *Remote Sens.* **2023**, *15*, 3560. [CrossRef]
5. Pasternak, F.; Bernard, P.; Georges, L.; Pascal, V. The microcarb instrument. In *International Society for Optics and Photonics, Proceedings of the International Conference on Space Optics—ICSO 2016, Biarritz, France, 18–21 October 2016*; Cugny, B., Karafolas, N., Sodnik, Z., Eds.; SPIE: Paris, France, 2017; Volume 10562, p. 105621P. [CrossRef]
6. Bojinski, S.; Verstraete, M.; Peterson, T.C.; Richter, C.; Simmons, A.; Zemp, M. The Concept of Essential Climate Variables in Support of Climate Research, Applications, and Policy. *Bull. Am. Meteorol. Soc.* **2014**, *95*, 1431–1443. [CrossRef]
7. Stephens, G.L.; Li, J.; Wild, M.; Clayson, C.A.; Loeb, N.; Kato, S.; L'Ecuyer, T.; Stackhouse, P.W.; Lebsock, M.; Andrews, T. An update on Earth's energy balance in light of the latest global observations. *Nat. Geosci.* **2012**, *5*, 691–696. [CrossRef]
8. Arvesen, J.C.; Griffin, R.N.; Pearson, B.D. Determination of extraterrestrial solar spectral irradiance from a research aircraft. *Appl. Opt.* **1969**, *8*, 2215–2232. [CrossRef] [PubMed]
9. Ångström, A. Apparent solar constant variations and their relation to the variability of atmospheric transmission. *Tellus* **1970**, *22*, 205–218. [CrossRef]
10. Shaw, G.E. Sun Photometry. *Bull. Am. Meteorol. Soc.* **1983**, *64*, 4–10. [CrossRef]
11. Gröbner, J.; Kerr, J.B. Ground-based determination of the spectral ultraviolet extraterrestrial solar irradiance: Providing a link between space-based and ground-based solar UV measurements. *J. Geophys. Res.* **2001**, *106*, 7211–7218. [CrossRef]
12. Harrison, L.; Kiedron, P.; Berndt, J.; Schlemmer, J. Extraterrestrial solar spectrum 360–1050 nm from rotating shadowband spectroradiometer measurements at the Southern Great Plains (ARM) site. *J. Geophys. Res. Atmos.* **2003**, *108* . [CrossRef]
13. Menang, K.P.; Coleman, M.D.; Gardiner, T.D.; Ptashnik, I.V.; Shine, K.P. A high-resolution near-infrared extraterrestrial solar spectrum derived from ground-based Fourier transform spectrometer measurements. *J. Geophys. Res. Atmos.* **2013**, *118*, 5319–5331. [CrossRef]
14. Bolsée, D.; Pereira, N.; Decuyper, W.; Gillotay, D.; Yu, H.; Sperfeld, P.; Pape, S.; Cuevas, E.; Redondas, A.; Hernandéz, Y.; et al. Accurate Determination of the TOA Solar Spectral NIR Irradiance Using a Primary Standard Source and the Bouguer-Langley Technique. *Sol. Phys.* **2014**, *289*, 2433–2457. [CrossRef]
15. Gröbner, J.; Kröger, I.; Egli, L.; Hülsen, G.; Riechelmann, S.; Sperfeld, P. The high-resolution extraterrestrial solar spectrum (QASUMEFTS) determined from ground-based solar irradiance measurements. *Atmos. Meas. Tech.* **2017**, *10*, 3375–3383. [CrossRef]
16. Elsey, J.; Coleman, M.D.; Gardiner, T.; Shine, K.P. Can Measurements of the Near-Infrared Solar Spectral Irradiance be Reconciled? A New Ground-Based Assessment Between 4000 and 10,000 cm^{-1}. *Geophys. Res. Lett.* **2017**, *44*, 10071–10080. [CrossRef]
17. Pereira, N.; Bolsée, D.; Sperfeld, P.; Pape, S.; Sluse, D.; Cessateur, G. Metrology of solar spectral irradiance at the top of the atmosphere in the near infrared measured at Mauna Loa Observatory: The PYR-ILIOS campaign. *Atmos. Meas. Tech.* **2018**, *11*, 6605–6615. [CrossRef]
18. Thuillier, G.; Hersé, M.; Labs, D.; Foujols, T.; Peetermans, W.; Gillotay, D.; Simon, P.; Mandel, H. The solar spectral irradiance from 200 to 2400 nm as measured by the SOLSPEC spectrometer from the ATLAS and EURECA missions. *Sol. Phys.* **2003**, *214*, 1–22. [CrossRef]
19. BenMoussa, A.; Gissot, S.; Schühle, U.; Del Zanna, G.; Auchère, F.; Mekaoui, S.; Jones, A.R.; Walton, D.; Eyles, C.J.; Thuillier, G.; et al. On-Orbit Degradation of Solar Instruments. *Sol. Phys.* **2013**, *288*, 389–434. [CrossRef]
20. Meftah, M.; Dominique, M.; BenMoussa, A.; Dammasch, I.E.; Bolsée, D.; Pereira, N.; Damé, L.; Bekki, S.; Hauchecorne, A. On-orbit degradation of recent space-based solar instruments and understanding of the degradation processes. In *Sensors and Systems for Space Applications X, Proceedings of the Society of Photo-Optical Instrumentation Engineers (SPIE) Conference Series, Anaheim, CA, USA, 2017* ; Pham, K.D., Chen, G., Eds.; SPIE: Paris, France, 2017; Volume 10196, p. 1019606. [CrossRef]
21. Schöll, M.; de Wit, T.D.; Kretzschmar, M.; Haberreiter, M. Making of a solar spectral irradiance dataset I: Observations, uncertainties, and methods. *J. Space Weather Space Clim.* **2016**, *6*, A14. [CrossRef]
22. Walker, J.H. *Spectral Irradiance Calibrations*; US Department of Commerce, National Bureau of Standards: Gaithersburg, MD, USA, 1987; Volume 250.
23. Mielenz, K.D.; Saunders, R.D.; Parr, A.C.; Hsia, J.J. The 1990 NIST scales of thermal radiometry. *J. Res. Natl. Inst. Stand. Technol.* **1990**, *95*, 621. [CrossRef]
24. Taylor, B.N.; Kuyatt, C.E. *Guidelines for Evaluating and Expressing the Uncertainty of NIST Measurement Results*; US Department of Commerce, Technology Administration, National Institute of Standards and Technology: Gaithersburg, MD, USA, 1994; Volume 1297.

25. Crouzet, P.E.; Duvet, L.; De Wit, F.; Beaufort, T.; Blommaert, S.; Butler, B.; Van Duinkerken, G.; ter Haar, J.; Heijnen, J.; van der Luijt, K.; et al. Quantum efficiency test set up performances for NIR detector characterization at ESTEC. In Proceedings of the High Energy, Optical, and Infrared Detectors for Astronomy VI, Montréal, QC, Canada, 22–25 June 2014; Volume 9154, pp. 476–488.

26. Langley, S.P. *Research on Solar Heat and Its Absorption by the Earth's Atmosphere*; US Government Printing Office: Washington, DC, USA, 1884; Volume 15.

27. Kasten, F.; Young, A.T. Revised optical air mass tables and approximation formula. *Appl. Opt.* **1989**, *28*, 4735–4738. [CrossRef] [PubMed]

28. Bodhaine, B.A.; Wood, N.B.; Dutton, E.G.; Slusser, J.R. On Rayleigh optical depth calculations. *J. Atmos. Ocean. Technol.* **1999**, *16*, 1854–1861. [CrossRef]

29. Harrison, L.; Michalsky, J.; Berndt, J. Automated multifilter rotating shadow-band radiometer: An instrument for optical depth and radiation measurements. *Appl. Opt.* **1994**, *33*, 5118–5125. [CrossRef] [PubMed]

30. Liu, C.; Li, Y.; Gao, W.; Shi, R.; Bai, K. Retrieval of columnar water vapor using multispectral radiometer measurements over northern China. *J. Appl. Remote Sens.* **2011**, *5*, 053558. [CrossRef]

31. Thome, K.J.; Smith, M.W.; Palmer, J.M.; Reagan, J.A. Three-channel solar radiometer for the determination of atmospheric columnar water vapor. *Appl. Opt.* **1994**, *33*, 5811–5819. [CrossRef]

32. Bovensmann, H.; Burrows, J.; Buchwitz, M.; Frerick, J.; Noel, S.; Rozanov, V.; Chance, K.; Goede, A. SCIAMACHY: Mission objectives and measurement modes. *J. Atmos. Sci.* **1999**, *56*, 127–150. [CrossRef]

33. Thuillier, G.; Harder, J.; Shapiro, A.; Woods, T.; Perrin, J.M.; Snow, M.; Sukhodolov, T.; Schmutz, W. SOLSPEC investigation on board the International Space Station: The Absolute Solar Spectral Irradiance in the Infrared Domain. In Proceedings of the EGU General Assembly Conference Abstracts, Vienna, Austria, 12–17 April 2015; p. 9663.

34. Harder, J.W.; Lawrence, G.M.; Rottman, G.J.; Woods, T.N. Spectral Irradiance Monitor (SIM) for the SORCE mission. In Proceedings of the Earth Observing Systems V, San Diego, CA, USA, 2–4 August 2000; Volume 4135, pp. 204–214.

35. Hilbig, T.; Weber, M.; Bramstedt, K.; Noël, S.; Burrows, J.; Krijger, J.; Snel, R.; Meftah, M.; Damé, L.; Bekki, S.; et al. The new SCIAMACHY reference solar spectral irradiance and its validation. *Sol. Phys.* **2018**, *293*, 1–26. [CrossRef]

36. Avrett, E.H. The solar temperature minimum and chromosphere. In Proceedings of the Current Theoretical Models and Future High Resolution Solar Observations: Preparing for ATST, Sunspot, NM, USA, 11–15 March 2002; Volume 286, p. 419.